

Dilek Funda Kurtulus¹, Berkan Anilir¹, Daniel Raymer²

¹Middle East Technical University, Aerospace Engineering Department, Ankara, Turkey. ²Conceptual Research Corp., Playa del Rey, CA, USA

Abstract

This paper unveils a numerical simulation of the aerodynamic characteristics of crescent wings across a range of high Reynolds numbers varying from 2×107 to 4×107. The study also explores the influence of the crescent wing's zero-sweep line on its aerodynamic performance. The wing sections of all models are NACA64A-010 airfoils. The turbulent flow is resolved by $k-\omega$ SST turbulence model. The methodology involves a validation process, aligning numerical simulations with wind tunnel experiments documented in existing literature, and they are in close agreement. The results indicate that all wings show sensitivity to Reynolds number variation. As the Reynolds number increases, the lift-to-drag ratio increases whereas the parasite drag decreases. Moreover, the maximum lift-to-drag ratio and parasite drag of the crescent wings are close to each other. On the other hand, the elliptic wing exhibits a lower lift-to-drag ratio and higher parasite drag characteristics. Oswald's efficiency factor values are greater than 0.9 at α =4°. As evident in the vorticity field and sectional aerodynamic coefficients, the flow separation near the wing tip is observed at α =10° for all wings except the elliptical one at Reynolds number of 2×10⁷ to 3×10⁷. The severity of this separation considerably increases at 4×10⁷ as it emerges the rise in the sudden peak of the sectional drag coefficient. This smooth separation characteristic of the elliptic wing leads to significantly lower induced drag than the crescent wings.

Keywords: Crescent wing, Elliptical wing, Oswald's efficiency factor, Computational Fluid Dynamics

1. Introduction

The crescent wing, characterized by its curved and tapered design reminiscent of a crescent moon, represents a departure from traditional straight and swept-back wing geometries. The elliptical crescent wings are identical to the elliptic wings except for highly swept wing tips. Since this shape is widely observed in nature, for example, the wing of common swift [1] and the tail of swordfish [2], the researchers considered that this wing should provide enhanced aerodynamic characteristics then they began to analyze it. According to van Dam's [3] low-order panel method solutions, the high aspect ratio moon-shaped crescent wing with 1.5c zero wing sweep produces 8% less induced drag than the straight leading edge elliptic wing. However, the wind tunnel experiments at Reynolds number of 1.7×10⁶ reveal that the gain in Oswald efficiency factor remains in the order of 3% (van Dam et al. [4]). Moreover, the lift-curve slope is not affected by the platform shape, but the stall angle of attack of the crescent wing is around 2° greater than the elliptic wing (van Dam et al. [5]). Mineck and Vijgen [6] conducted the experiments in Langley 8-foot Transonic Pressure Tunnel at Reynolds numbers of 2.1×10⁶ and 3×10⁶. An interesting result shows that the lift-curve slope and Oswald efficiency factor of the unswept trailing edge wing are greater than the 0.25c and 1.50c sweep wings, even though it has a sweep in between the other two. In another wind tunnel experiment conducted by Lazos [7], the crescent wing with 2c zero-sweep is superior to the straight trailing edge elliptic wing in terms of efficiency factor and lift-to-drag ratio at a Reynolds number of about 0.3×106. Ardonceau's [8] wind tunnel tests at Reynolds number of 0.55×106 also pointed out that the stall

angle enhances as the sweep increases. On the other hand, he found a reduction in the efficiency factor for crescent wings.

Dr. Raymer has been researching the use of superellipse mathematics for defining wing planforms. The typical crescent wings as seen in nature and various aerodynamic research papers can be closely approximated by swept superelliptical planforms with the sweep angle defined aft of the trailing edge. Using this mathematics, apparently complicated crescent wing planforms can be exactly defined with just a few input parameters.

On behalf of the studies mentioned above, there is a gap in the literature that the studies on the elliptical crescent wings are limited to the highest Reynolds number 3.0×10^6 . Also, the higher number of zero-sweep lines between 0c and 1.5c could be examined. Therefore, the main objective of the current study is to numerically investigate the aerodynamic characteristics of the elliptical crescent wings in terms of aerodynamic coefficients, induced drag, and Oswald's efficiency factor at Reynolds numbers between 2×10^7 and 4×10^7 . Further, the influence of various zero-sweep lines (S_0) on aerodynamic characteristics will be examined.

The structure of this paper is as follows: the details of problem setup, wing geometries, numerical method, computational domain, and grid refinement study are given in Section 2. The results of numerical simulations are presented in Section 3 as, validation of simulations in Section 3.1, general observations on the aerodynamic coefficients in Section 3.2, and examination of flow formation and distribution of sectional lift and drag coefficients along the wing span in Section 3.3. Finally, Section 4 concludes the study.

2. Methodology

2.1 Problem Setup

In this paper, the influence of a crescent wing platform shape specifying a zero-sweep line at various percentages of the chord on the aerodynamic characteristics is examined. Figure 1 presents the family of elliptical crescent wings with different zero-sweep lines. The wings are generated by Raymer's RDS^{win}-Pro aircraft design software in a specially-coded routine [9]. Throughout the paper, the wing with zero-sweep line at 0.30c will be mostly called as elliptic wing, and the other wings as crescent wings. The half-wing model is simulated by prescribing the symmetry boundary condition at the root. The root chord and semi-span are set to 5.01 m and 11.80 m, respectively. The mean aerodynamic chord is obtained at about 4.1 m. All wings have a wing area of 46.45 m² and a semi-aspect ratio of 3. No incidence, twist, or dihedral is included. The generic 0.10c thickness NACA64A-010 airfoil is used. The x coordinate of the tip is defined by the leading edge eccentricity and provides the crescent shape. The exponent of the elliptic chord distribution is x=2. The present wing geometries have rounded trailing edges and cut wingtip. The details of the dimensions are provided in Figure 2.

The simulations are performed at sea-level standard atmospheric conditions with ranging freestream Mach numbers (M) between 0.2 and 0.4. The corresponding minimum and maximum Reynolds numbers based on freestream velocity and mean aerodynamic chord length are 2×10^7 and 4×10^7 , respectively. The ideal gas assumption is applied with Sutherland's law to calculate airflow properties.

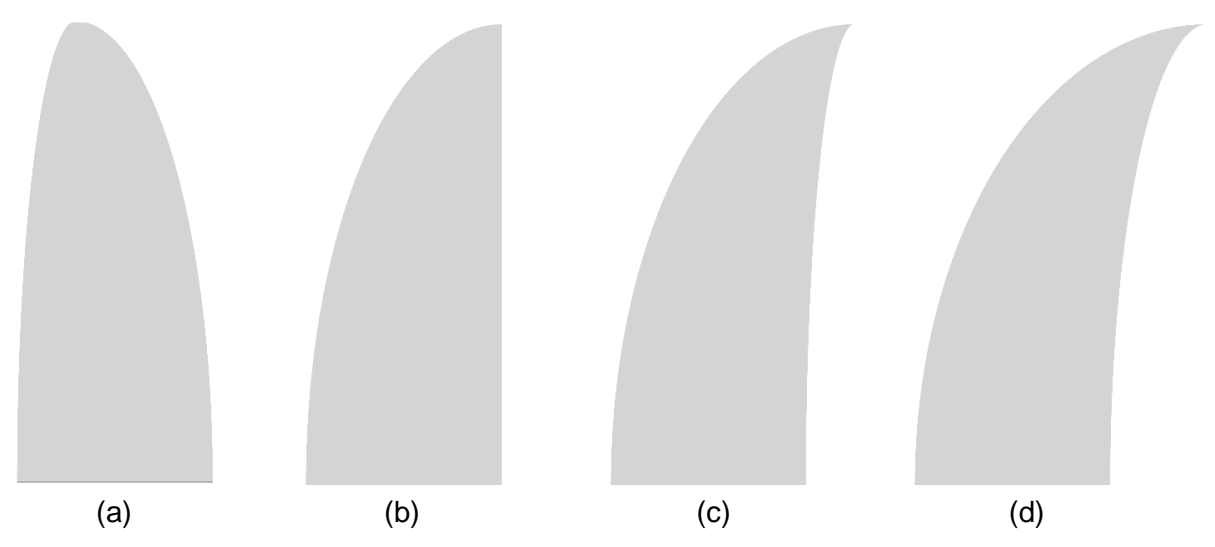


Figure 1 – Top view of elliptical crescent wing geometries with a zero-sweep line at (a) 0.30c (elliptic wing), (b) 1c, (c) 1.25c, and (d) 1.50c

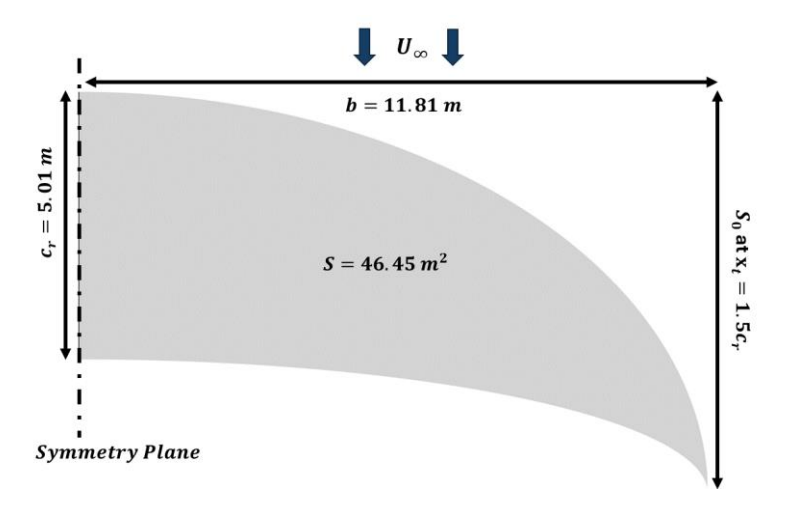


Figure 2 – Problem setup for crescent wing

The efficiency of the wing is defined by means of the Oswald efficiency factor by Eq.(1) and Eq.(2) [10].

$$C_D = C_{D_0} + C_{Di} \tag{1}$$

$$e = \frac{C_L^2}{\pi ARC_{Di}} \tag{2}$$

where C_D , C_{D0} and C_{Di} are the total drag coefficient, parasite drag coefficient (drag coefficient at zero-lift) and induced drag coefficient, respectively. C_L is the lift coefficient, e is the Oswald's efficiency factor, and AR is the aspect ratio of the wing.

2.2 Numerical Method

The three-dimensional compressible flow over the elliptical wings is simulated numerically with a commercial finite volume solver of ANSYS Fluent v17.2 [11] by solving Reynolds-averaged Navier-Stokes (RANS) equations. The numerical solution is obtained by evaluating the gradients using the Least Squares Cells-Based scheme. The second-order upwind scheme was adopted as the method to discretize pressure, momentum, turbulent kinetic energy, and specific dissipation rate. Pressure-velocity coupling is done by a Coupled algorithm, and the details of the algorithm can be found in Ferziger et al. [12]. Menter's [13] $k-\omega$ SST (Shear-Stress Transport) turbulence model is used to comprise the turbulence effect on the numerical simulations. This turbulence model uses $k-\omega$ model in the inner-wall regions to capture the sub-viscous layer effects, and $k-\varepsilon$ model in the outer portion

of the boundary layer. The blending function procures the transition between the models, and this function is designed to activate the standard $k-\omega$ model and $k-\varepsilon$ model in the near-wall and away-wall regions, respectively [13, 14].

The grids are generated in the Pointwise V18.5R1 program. The mesh is composed of different parts. T-Rex (3D anisotropic tetrahedral extrusion) method is used to resolve the boundary layer. It extends an unstructured hexahedra cell with a growth rate of 1.15 until it reaches an isotropic height of 0.85 of the wing surface mesh. The total number of cells at the boundary layer is approximately 14×10^6 , which corresponds to half of the whole computational domain. The space between the boundary layer and the farfield is filled up with axis-aligned regular hexahedra (called Voxel) cells, while the transition between different-sized hexahedra cells is achieved using combinations of tetrahedra and pyramid cells. The wake region of the wing is refined to capture flow properties there for each analyzed angle of attack case. Then, the total number of elements is equal to about 28×10^6 . The origin is specified at the leading edge of the root airfoil (at y=0 plane). The computational domain covers the largest domain being $(x/c, y/c, z/c) \in [-15, 15] \times [0, 15] \times [-15, 15]$, where x, y, and z are the streamwise, spanwise, and vertical coordinates, respectively. The surface mesh of the wing can be seen in Figure 3. The noslip boundary condition (wall) is applied to the wing surface, and the outer domain is assigned as the pressure farfield.

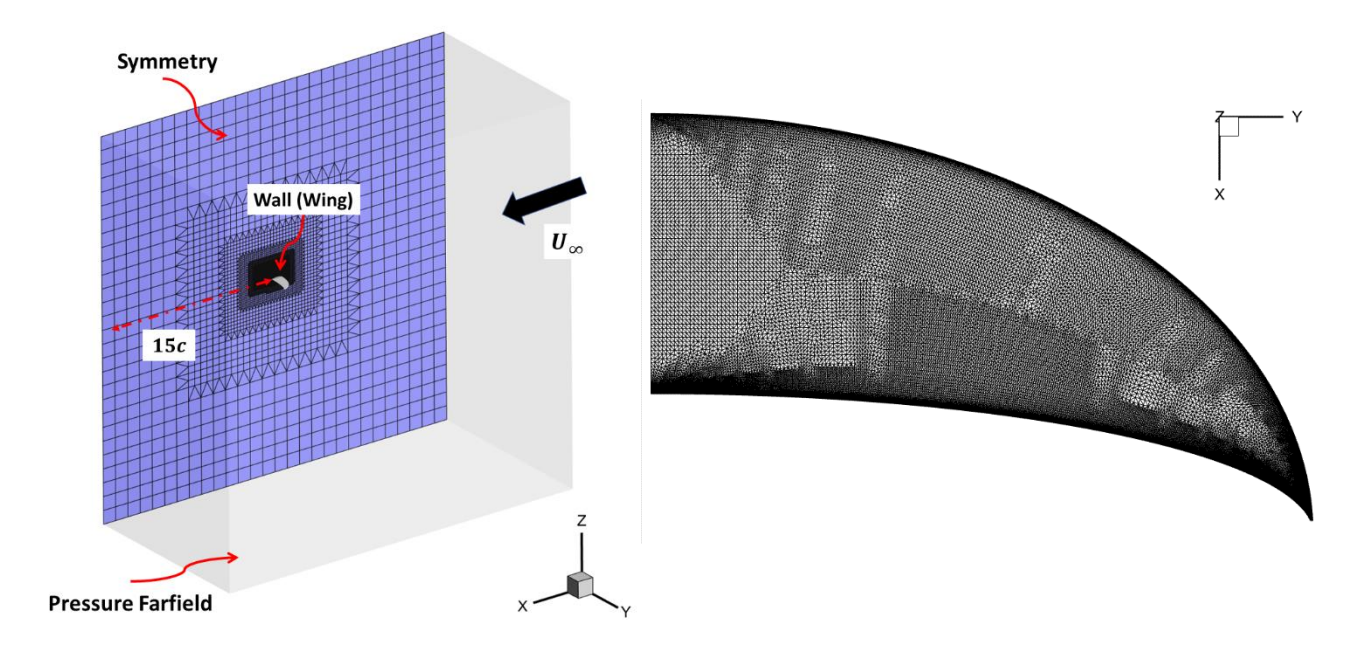
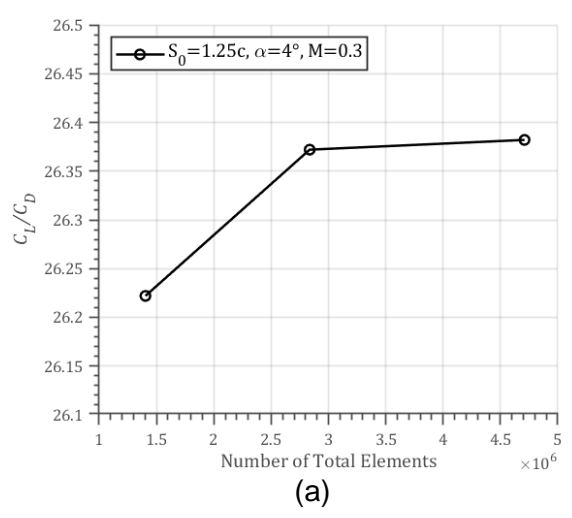


Figure 3 – Boundary conditions, computational domain, and surface mesh of the crescent wing

2.3 Grid Refinement Study

Grid refinement study was performed for a flow over the crescent wing with S_0 =1.5 at angles of attack of 4° and 10° to obtain the comparison of the aerodynamic coefficients. Three different grids, named coarse, medium, and fine grids, were employed with a refinement ratio of around 2 applied on the points around the surface grid of the wing. The coarse, medium, and fine grids contain approximately 15×10° elements, 28×10° elements, and 47×10° elements, respectively. Figure 4 shows the comparison of the lift-to-drag ratio of different grids. The results obtained from the medium grid are in very good agreement against the fine grid with less than 1% errors at both analyzed angles of attack. Therefore, the rest of the study was performed with the medium grid.



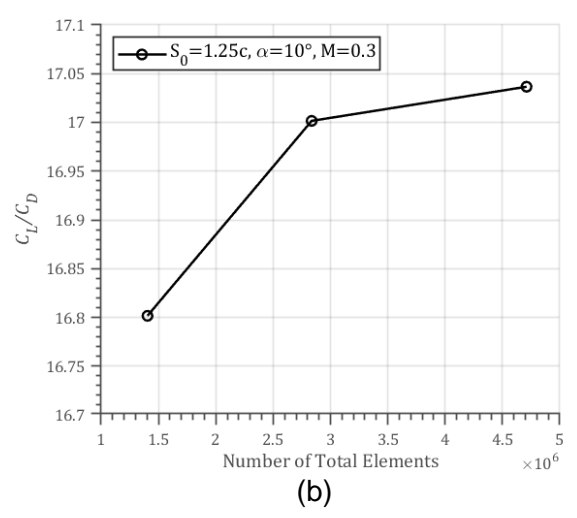


Figure 4 – Comparison of various levels of grids in terms of lift-to-drag ratio for S_0 =1.5 wing at angles of attack of (a) 4° and (b) 10°

3. Results and Discussion

3.1 Validation Study

The numerical simulations are validated against the published wind tunnel experiments of van Dam et al. [4] on the crescent wing planform shown in Figure 5. The airfoil used for this experimental wing was NACA 0012 airfoil. The experiments were carried out in the NASA Langley 14 ft ×22 ft subsonic tunnel at a Reynolds number of about 1.7×10⁶ and Mach number of 0.27 for wide range of angles of attack that contain pre and post-stall conditions. In the experiment, the wing was mounted on the cylindrical fuselage, and the fairing was installed in order to smooth the flow near the fuselage wing interference region. Moreover, the configurations of high wing and low wing were tested, and both of their results are provided in Figure 6. In the present numerical simulations, the wing platform was drawn without the fuselage and the fairing, as a clean configuration.

Figure 6 shows the comparison of the wind tunnel experiments and the numerical simulations in terms of aerodynamic coefficients. The numerical results are in good agreement with the experimental results prior to stall. The lift curves show a linear behavior until the stall, and the lift curve slope is obtained as approximately 1.47π . On the other hand, the stall angle of attack predicted by numerical simulations is very close to the elliptical wing results, but it is about 3° less than the experiment on the high wing configuration. This apparently influences the maximum lift coefficient values. The value and the angle of the maximum lift-to-drag ratio are satisfactorily predicted by the numerical simulations.

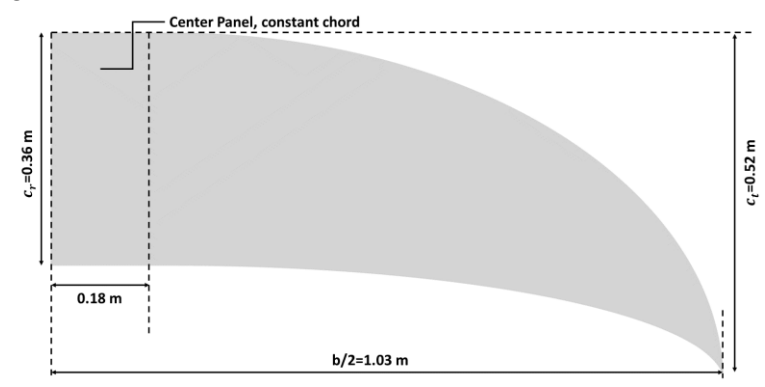


Figure 5 – Top view of the crescent wing platform of van Dam et al. [4] used in the validation study with NACA0012 airfoil as a cross-sectional profile

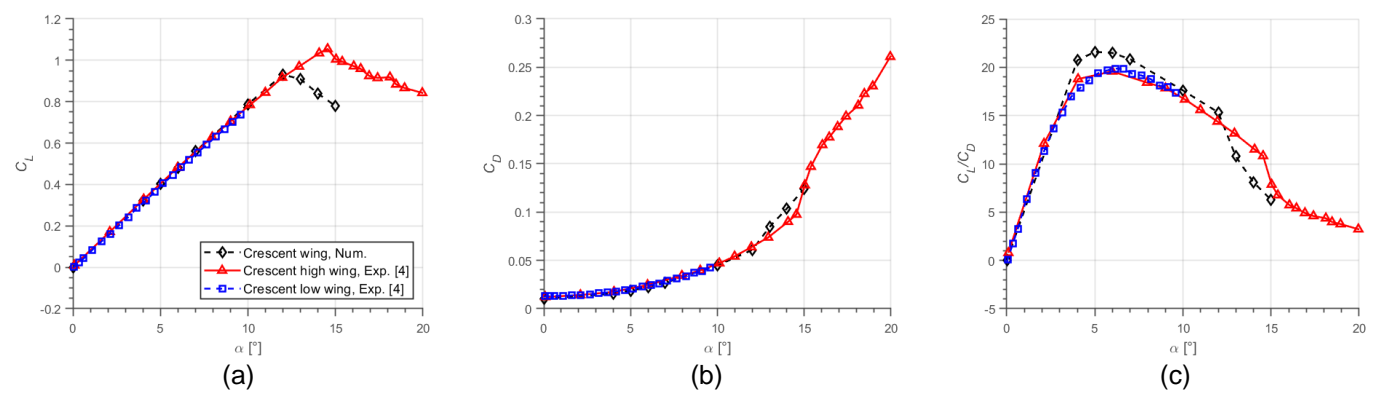


Figure 6 – Comparison of the numerical simulations with van Dam et al. [4]'s wind tunnel experiments (a) lift coefficient, (b) drag coefficient, and (c) lift-to-drag ratio

3.2 General Observations in terms of Aerodynamic Coefficients

Figure 7a reveals the influence of Reynolds number and zero-sweep line on the maximum lift-todrag ratio $(C_L/C_D)_{max}$. For all four wings and three Reynolds numbers, the maximum-lift-to-drag ratio is achieved at α =4°. Also, a general trend of almost linearly increasing maximum-lift-to-drag ratio with Reynolds number is observed. The crescent wing with straight trailing edge (S_0) exhibits a marginally higher $(C_L/C_D)_{max}$ than other crescent wings. Furthermore, the elliptic wing produces noticeably lower $(C_L/C_D)_{max}$ than other wing regardless of Reynolds number. Van Dam et al. [4]'s wind tunnel experiments also show that the S_0 =1.5c crescent wing leads to slight improvement in $(C_L/C_D)_{max}$ compared to elliptical wing. Another important aerodynamic parameter for the performance of the wing is parasite drag (C_{D0}). Usually referred to as parasite drag or zero-lift drag, these drag forces do not have a strong relationship to lift. When a well-built aircraft cruises at subsonic speeds, skin-friction drag accounts for the majority of the parasite drag, which is mostly dependent on the wetted area. Since the wings are constructed with symmetrical airfoil, the parasite drag value is obtained at α =0° where the lift and hence induced drag are 0. The C_{D0} values for all wings tested are observed to be approximately 0.006–0.007 over the Reynolds numbers tested. C_{D0} is gradually decreases as the Reynolds number increases (Figure 7b). Obviously, the reason behind this is the decrease in the dominance of the viscosity at higher Reynolds numbers. It is noticed that the elliptic wing produces higher parasite drag than the other wings. The backward-sweep (higher S_0) leads to improvement in C_{D0} .

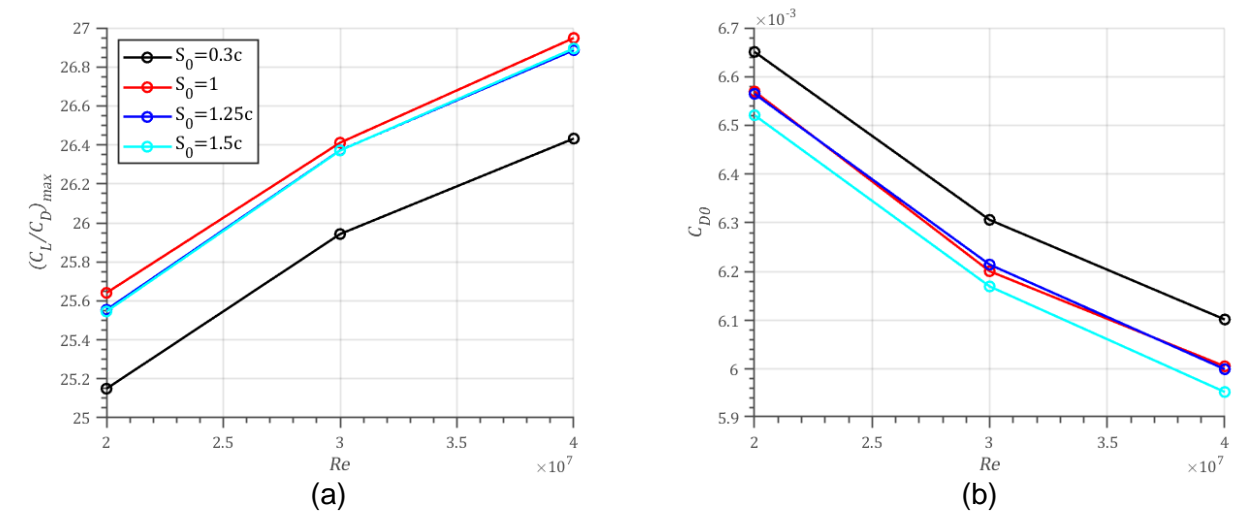


Figure 7 – Variation of (a) maximum lift-to-drag ratio and (b) parasite drag coefficient with respect to Reynolds number and S_0

Figure 8 presents induced drag and Oswald's efficiency factor as a function of Reynolds number at α =4° and α =10°. The induced drag is component of drag literally caused by the creation of lift, hence also called as drag-due-to-lift [10, 15]. For both two examined angles of attacks, the induced drag increases with increasing Reynolds number. The induced drag is found for all wings tested to be in

the range of 5.5×10^{-3} to 6.1×10^{-3} at α =4°, and these values are very close to parasite drag at the same condition. The straight trailing edge crescent wing (S_0) produces higher induced drag but has higher Oswald's efficiency than other wings at α =4°. The reason could be attributed to have higher lift force, for instance, the lift coefficients of S_0 =0.3c, 1c, 1.25c, and 1.5c at α =4° and Re=3×10⁷ equal to 0.311, 0.317, 0.315 and 0.312, respectively. If the higher angle of attack of α =10° is examined, it is noticed a striking feature that the induced drag is almost independent of the zero-sweep line for crescent wings, but the elliptic wing produces considerably less. The reasons behind this will be detailly discussed in the following section, but it can be mentioned that the crescent wings exhibit separated flow near the wing-tip similar to high tapered wings and the induced drag also includes drag due to viscous separation. On the other hand, the flow is fully attached for an elliptic wing at α =10° except Re=4×10⁷.

The general trend for Oswald's efficiency factor can be summarized as follows: if the flow is attached, variation of e with respect to Reynolds number exhibits an almost insignificant rise, for instance, the results at α =4°. On the other hand, if the separation over the wing takes place, it becomes stronger with increasing Reynolds number then e reduces. For instance, the flow is attached for elliptic wing at α =10°, Re=2×10⁷ and Re=3×10⁷ thus e does not change with Reynolds number (Figure 8b). Nevertheless, the crescent wings experience the separation at α =10° for each Reynolds number, therefore e considerably decreases as Reynolds number increases. The typical and commonly recommended e values in the literature are between 0.7-0.85 [10, 18]. Since the analyzed wings are elliptical, the e values are above 0.9 and the maximum e is achieved for S_0 =1c at Re=4×10⁷ as e=0.926.

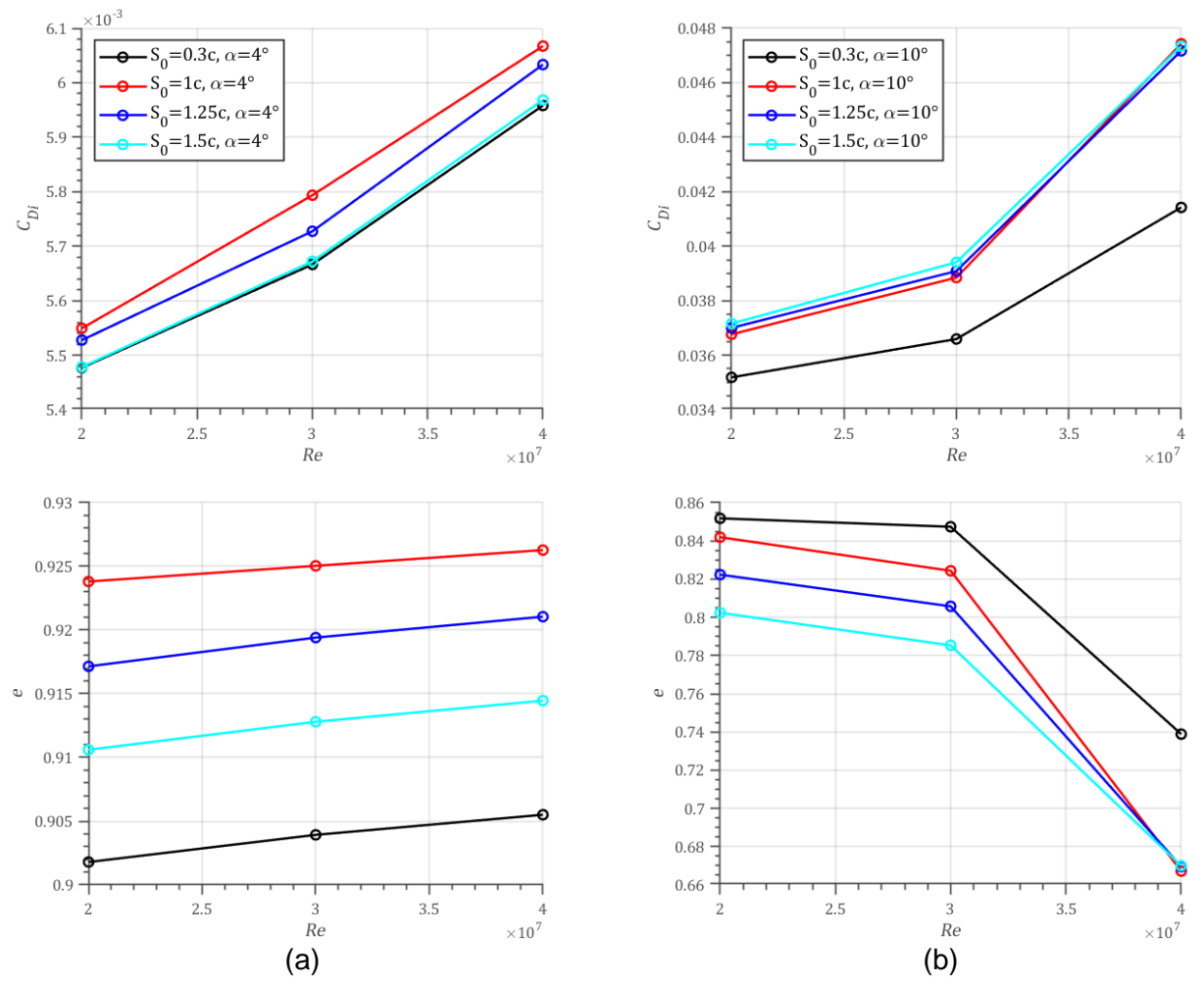
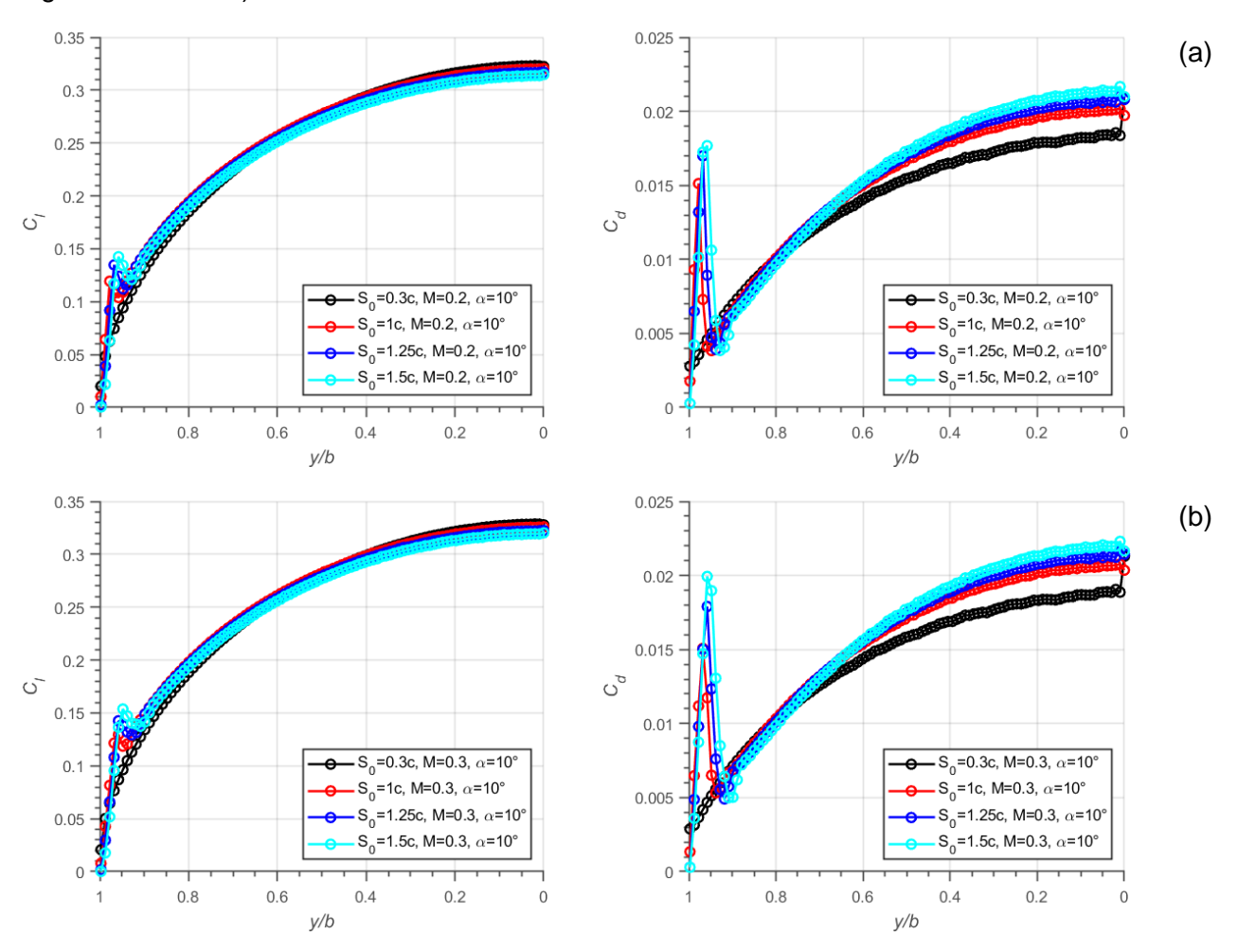


Figure 8 Variation of induced drag and Oswald's efficiency factor at angles of attack of (a) 4° and (b) 10° with respect to Reynolds number and S_0

3.3 Examination of Flow Structure and Sectional Aerodynamic Coefficients

In this section, the flowfield over the wings is examined by observing the vorticity field and distribution of lift and drag coefficient along the wing span. In order to obtain the sectional lift (C_l) and drag (C_d) coefficients, we initially took 100 cross section slices along the wing span. Then, the integral of pressure and wall shear stress over these slices towards the freestream direction and perpendicular direction gives the resultant drag and lift forces, respectively [16]. Finally, these forces are nondimensionalized with dynamic pressure $(0.5\rho U_{\infty})$ and wing span (b).

Let us explore the influence of S_0 on the sectional aerodynamic coefficients. Figures 9a to 9c depict the variation of sectional lift coefficients along the spanwise direction at α =10° (y/b=0 and y/b=1 refer to root and tip sections). The main difference between the wings' aerodynamics is not observed on the lift but drag, thus we will more closely examine \mathcal{C}_d distribution. Both \mathcal{C}_l and \mathcal{C}_d gradually decrease from wing root to wing tip except the separation region. The separation emerges itself as a sudden rise in C_d . For all wings, if the separation is observed, it occurs near the wing tip similar to those high tapered wings. Regardless of Reynolds number, the higher S_0 leads to less C_l and greater C_d from wing root to y/b=0.6. The elliptic experiences the fully attached flow at $Re=2\times10^7$, and $Re=3\times10^7$ and much smoother but discrete separation than that crescent wings at $Re=4\times10^7$. This finding coincides with previous results that the induced drag penalty of the elliptic wing is much lower (see Figure 8b). For crescent wings, the peak C_d of S_0 =1.5c is greater than other wings for each analyzed Reynolds number. Moreover, C_d exhibits a peak very near to wing tip at around y/b=0.96for $Re=2\times10^7$, and $Re=3\times10^7$ regardless of S_0 . As the Reynolds number and Mach number are increased further to $Re=4\times10^7$ and M=0.4 where the compressibility effects can not be neglected, the separation moves towards to wing root (peaks at y/b=0.88) and becomes more severe (see Figure 9c and 10d).



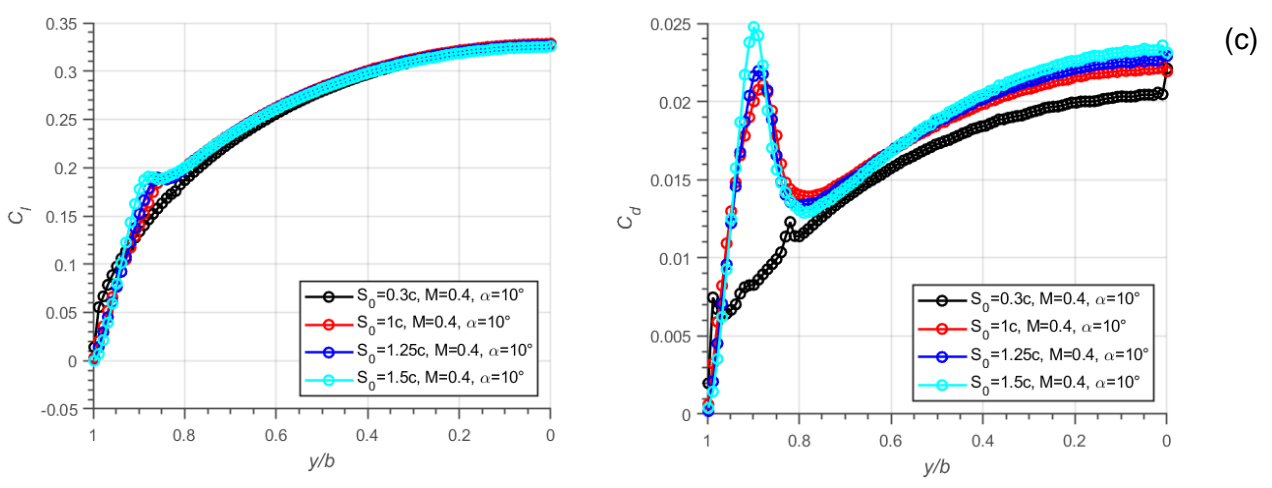


Figure 9 – Distribution of sectional lift and drag coefficients along the wing span with respect to S_0 at $\alpha=10^\circ$, (a) $Re=2\times10^7$, (b) $Re=3\times10^7$, and (c) $Re=4\times10^7$

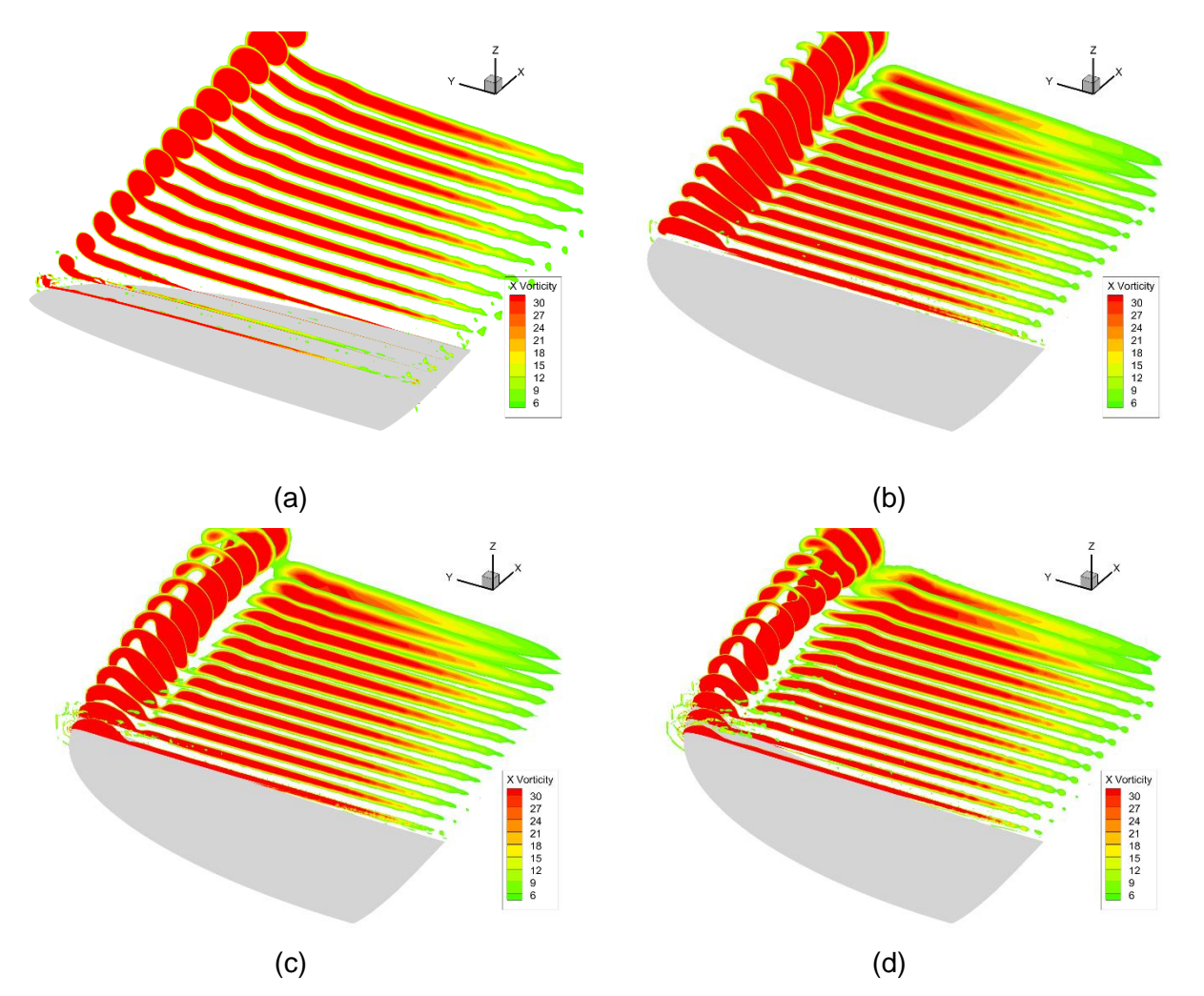


Figure 10 – X Vorticity contours in the wake of (a) S_0 =0.3c, (b) S_0 =1c, (c) S_0 =1.25c, and (d) S_0 =1.5c at α =10° and Re=4×10⁷

4. Conclusion

The numerical simulations are conducted to explore the aerodynamic characteristics of different zero-sweep line elliptical crescent wings at high Reynolds numbers ranging from 2×10^7 (M = 0.2) to 4×10^7 (M = 0.4). These zero-sweep lines are specified as 0.3c (elliptic wing), 1c, 1.25c, and 1.5c. The wings are half-model wings, in which the symmetry boundary condition is prescribed at the root, and they are generated by Raymer's RDS^{win}-Pro aircraft design software in a specially-coded routine. The exponent of the elliptic chord distribution and the semi-aspect ratio of the wings are n = 2 and n = 2

respectively.

The commercial finite volume solver of ANSYS Fluent v17.2 is used to simulate the flowfield and the turbulent flow is resolved by $k-\omega$ SST turbulence model. The grid refinement study is conducted to obtain the optimal grid for the crescent wing with S_0 =1.5 at angles of attack of 4° and 10°. This study shows that the results of medium and fine grids are very close to each other. Therefore, the rest of the simulations are performed with a medium grid that contains 28×10⁶ number of elements.

The numerical simulations undergo validation against wind tunnel experiments of van Dam et al. [4] for S_0 =1.5 wing, demonstrating a good concurrence in terms of lift coefficient, drag coefficient, and lift-to-drag ratio. On the comparison of the wings, there is no influence of the zero-sweep line on the angle of attack where the maximum lift-to-drag ratio is achieved. On the other hand, the elliptic wing results in a slightly lower maximum lift-to-drag ratio than the crescent wings. The parasite drag characteristic is slightly improved as the wing is swept more. For induced drag and Oswald's efficiency factor at α =4°, the straight trailing edge crescent wing (S_0 =1c) leads to higher quantities than other wings. Also, Oswald's efficiency factor values are greater than 0.9. The maximum lift-to-drag ratio, induced drag, and Oswald's efficiency factor enhance as the Reynolds number increases whereas the parasite drag decreases.

As the sectional aerodynamic coefficients emerge, the flow separation near the wing tip is observed at α =10° for all wings except the elliptical one at Reynolds number of 2×10⁷ to 3×10⁷. Although the elliptic wing exhibits much smoother but discrete separation, the severity of this separation considerably increases at 4×10⁷ for crescent wings.

5. Contact Author Email Address

Corresponding author's email adress: anilir.berkan@metu.edu.tr

6. Copyright Statement

The authors confirm that they, and/or their company or organization, hold copyright on all of the original material included in this paper. The authors also confirm that they have obtained permission, from the copyright holder of any third party material included in this paper, to publish it as part of their paper. The authors confirm that they give permission or have obtained permission from the copyright holder of this paper, for the publication and distribution of this paper as part of the ICAS proceedings or as individual off-prints from the proceedings.

References

- [1] Lighthill, M. J. Swimming and Flying in Nature. Berlin, Springer, pp.423-491, 1975.
- [2] Sagong, W., Jeon .W.-P. and Choi H. Hydrodynamic Characteristics of the Sailfish (Istiophorus platypterus) and Swordfish (Xiphias gladius) in Gliding Postures at Their Cruise Speeds. *PLoS ONE*, Vol. 8, No. 12, pp. e81323, 2013.
- [3] Van Dam, C. P. Induced-Drag Characteristics of Crescent-Moon-Shaped Wings. *Journal of Aircraft*, Vol. 24, No. 2, pp 115-119, 1987.
- [4] Van Dam, C. P., Vijgen P. M. H. W. and Holmes, B. J. Experimental Investigation on the Effect of Crescent Planform on Lift and Drag. *Journal of Aircraft*, Vol. 28, No. 11, pp 713-720, 1991.
- [5] Van Dam, C. P., Vijgen P. M. H. W. and Holmes, B. J. Aerodynamic Characteristics of Crescent and Elliptic Wings at High Angles of Attack. *Journal of Aircraft*, Vol. 28, No. 4, pp 253-260, 1991.
- [6] Mineck, R. E. and Vijgen P. M. H. W. Wind-Tunnel Investigation of Aerodynamic Efficiency of Three Planar Elliptical Wings with Curvature of Quarter-Chord Line, *NASA Technical Paper* 3359, 1993.
- [7] Lazos, B. S. Biologically Inspired Fixed-Wing Configuration Studies. *Journal of Aircraft*, Vol. 42, No. 5, pp 1089-1098, 2005.
- [8] Ardonceau, P. L. Aerodynamic Properties of Crescent Wing Planforms. *Journal of Aircraft*, Vol. 31, No. 2, pp. 462-465, 1994.
- [9] Raymer, D. RDS^{win}: Seamlessly-Integrated Aircraft Conceptual Design for Students & Professionals. *54th AIAA Aerospace Sciences Meeting*, San Diego, CA, January 2016.

- [10] Raymer, D. P. Aircraft Design: a Conceptual Approach, 6th ed., Washington, D.C., USA, 2018.
- [11] ANSYS Inc. ANSYS Fluent User's Guide, Release 17.2, 2016.
- [12] Ferziger, J. H., Peric M. and Street R. L. *Computational Methods for Fluid Dynamics*. 4th ed., Springer, Switzerland, 2020.
- [13] Menter, F R., Two-Equation Eddy-Viscosity Turbulence Models for Engineering Applications. *AIAA Journal*, Vol. 32, No. 8, pp 1598–1605, 1994.
- [14] Wilcox, D C., Turbulence Modeling for CFD, 3rd ed., DCW Industries, Inc., La Cañada, California, 2006.
- [15] Spedding, G R., and McArthur, J. Span Efficiencies of Wings at Low Reynolds Numbers, *Journal of Aircraft*, Vol. 47, No.1, pp. 120-128, 2010.
- [16] Anilir, B. and Kurtulus, D F., Pre- and Post-stall Characteristics of a Very Light Aircraft's Wing for Different Design Parameters, *Progress in Computational Fluid Dynamics*, Vol. 23, No.5, pp. 278-291, 2023.
- [17] Ananda G K., Sukumar, P P. and Selig M S. Measured Aerodynamic Characteristics of Wings at Low Reynolds Numbers, *Aerospace Science and Technology*, Vol. 42, pp. 392-406, 2015.